Chemical Engineering Journal 519 (2025) 165154

Contents lists available at ScienceDirect

Chemical Engineering Journal

journal homepage: www.elsevier.com/locate/cej

Novel bioelectrochemically assisted in situ pH modulation method for urea stabilization and phosphorus recovery from synthetic urine☆

Kristóf Bence Nagy [a], Mónika Meiczinger [b], Boglárka Bocska [a], Nándor Nemestóthy [a], László Koók [a,*]

[a] Research Group on Bioengineering, Membrane Technology and Energetics, University of Pannonia, Egyetem str. 10, Veszprém H-8200, Hungary
[b] Sustainability Solutions Research Lab, University of Pannonia, Egyetem str. 10, Veszprem H-8200, Hungary

ARTICLE INFO

Keywords:
Bioelectrochemical pH modulation
Microbial electrolysis cell
Phosphorus recovery
Synthetic urine
Urea stabilization

ABSTRACT

Urine is considered as excellent source of N and P. For efficient recovery of these compounds from urine, separate collection and transportation must be managed. However, urease enzyme, highly abundant in nature (and urine-treating systems), rapidly catalyses urea hydrolysis (main N-compound) to ammonia and carbonic acid, causing significant N-loss and odour issues. Thus, the stabilization of urea in urine is crucial for enabling its utilization as resource. In this study, a novel bioelectrochemically assisted pH modulation method in microbial electrolysis cells (MECs) is presented for efficient urea stabilization. Using synthetic urine catholyte in MEC, the cathodic OH^- production allowed urease inhibition at a threshold of pH $\geq$ 11. Experiments in internal cathode chamber MEC revealed reverse linear relationship between cathode surface area to catholyte volume ratio and required operation time to ensure pH = 11. Additional pH modulation experiments with optimized 3D-printed MEC showed that low current density (j = 1.43 A m^{-2}) leads to protracted pH increase (>1000 min), while efficient current generation (j = 4.6 and 5.4 A m^{-2}) led to rapid stabilization in 62 and 55 min, respectively. pH-treated samples remained stable over ~1 month and proved to be effective for urease inhibition in enzyme treatment test. Effective P-recovery achieved 66.7–96.5% of the theoretical maximum (limited by bivalent cations). Aspects of mass transport and pH splitting-related losses were discussed in context of process efficiency. The results highlight the applicability of bioelectrochemically-driven pH modulation as novel strategy for urea stabilization and nutrient recovery from urine.

1. Introduction

Source separated urine is a highly concentrated and inexhaustible nitrogen (and phosphorus) source, containing 70–80% of the total nitrogen excreted by humans, primarily in the form of urea ($CO(NH_2)_2$). Meanwhile, the increasing demand for nutrition raises economical and availability challenges for non-renewable N- and P-based fertilizer production. Therefore, practical implementation of technologies capable of collecting, transporting and treating urine for resource recovery should be urged [1]. However, urea is highly susceptible to enzymatic hydrolysis by urease-producing microorganisms, leading to rapid ammonia volatilization and nitrogen loss in urine collection and transportation systems [2,3] and thus, centralized urine processing and resource recovery strategies are mitigated [4,5]. This realization highlights the on-site urine treatment methods, among which, electrochemical techniques (e.g. stripping, in situ produced oxidative treatment, capacitive deionization or electrochemically induced precipitation) offer convenient solutions [6–9]. Unlike in case of using acidification agents, alkali dosing or external chemical inhibitors (i.e. techniques with additional chemical input and cost), the electrochemical approach is often more energy-efficient and sustainable.

So-called electrochemical pH modulation method was used for N- and P-recovery from wastewater [10,11]. It showed promising results also for the stabilization of urea in urine by achieving high enough pH values for urease inhibition and concurrent phosphate precipitation (in form of struvite, hydroxyapatite or Ca/Mg phosphate) driven by OH^- formation on the cathode of an electrochemical cell, according to Eq. 1 [9,11,12].

☆ This article is part of a Special issue entitled: 'Beyond the Horizon of MET' published in Chemical Engineering Journal.

* Corresponding author.
E-mail address: kook.laszlo@mk.uni-pannon.hu (L. Koók).

https://doi.org/10.1016/j.cej.2025.165154
Received 7 February 2025; Received in revised form 5 June 2025; Accepted 19 June 2025
Available online 20 June 2025

$$H_2O + e^- \rightarrow \frac{1}{2}H_2 + OH^- \quad (\epsilon^0 = -0.8227\ V\ vs.SHE) \tag{1}$$

For example, et al. [9] presented two- and three-chambered electrochemical systems, in which they could stabilize urea in urine for >18 months by precipitating phosphate and bivalent cations at pH = 12. Their work also evaluated the effect of various ion exchange membrane combinations on system performance. This approach stabilizes urea and allows collection and transportation for further (e.g. fertilizer) processing. Electrochemical methods for direct ammonia recovery also exists, although in that case, on-site treatment is needed [13]. The main challenge in electrochemical pH modulation seems to be the usage of supporting electrolytes (such as sodium sulphate), i.e. chemical dosing. Even though the produced stream usually can be further used, such as acidic streams for cleaning and descaling purposes in urine collection / treatment systems, electrochemical methods can be competitive only by exploiting their main advantage: the lack of need for excess chemical addition. Moreover, the energy requirement for simultaneous P-recovery in conventional electrochemical systems may be a limiting factor from diluted sources.

In a certain type of bioelectrochemical systems (BES), namely in microbial electrolysis cells (MEC), the joint effect of anodic oxidation of organics by electrochemically active (exoelectrogenic) bacteria, and the supported external energy (e.g. ≥ 0.2 V external voltage) drives low-current H_2 formation at the cathode, accompanied with OH^- formation [14]. Although the increasing alkalinity of the catholyte induces energetic losses in MEC and deteriorates the cell efficiency [15], exploiting this – mostly inevitable – side-effect of MEC operation opens the way for the development of an innovative, bioelectrochemically assisted pH modulation method by using urine as catholyte in the reactor. Thus, the (bio)electrochemically induced stabilization of urea – and potentially, the recovery of phosphorus – could be performed alongside the energy-efficient hydrogen production and organics (e.g. wastewater) degradation. This approach combines the benefits of simultaneous treatment of waste and urine in the anodic and cathodic compartments, while resolves the need of chemical dosing, as urine can be used as catholyte.

Despite the potential of MEC-based urea stabilization, significant research efforts have to be made to address the key questions this novel concept evokes. The main objectives of this study are to understand the interplay between bioelectrochemical activity, cathodic pH modulation kinetics, urea stabilization and P-recovery efficiency. These insights are essential for further process optimization. Furthermore, the present work will address the issues related to mass transport limitations and long-term stability, which are critical for pushing the technology for real urine treatment applications. Accordingly, this work investigates the feasibility of bioelectrochemically assisted urea stabilization in synthetic urine via cathodic pH modulation in MECs for the first time. The experimental approach presented here allows the evaluation of the effect of reactor design, electrode area to electrolyte volume ratios, operating conditions (catholyte type, current density) on the kinetics and efficiency of the bioelectrochemical pH modulation process, as well as on P-recovery and urea stability. In addition to conventional glass reactors, 3D-printed MEC design is also introduced in the present work. 3D-printing in MEC, and in general in BES is used to obtain biocompatible conductive functional elements, such as electrodes [16], and it was shown to allow rapid and efficient prototyping, scale-up and optimization [17,18]. Thus, we aim to provide novel and insightful information on a low-current bioelectrochemical platform with implications for decentralized urine treatment and nutrient recovery.

2. Materials and methods

2.1. Inoculum source and chemicals

MEC reactors were inoculated with 10 *V*/V % mesophilic anaerobic sludge collected from a biogas fermenter treating municipal wastewater. The chemicals used were at least of analytical grade. Sodium-acetate (≥99.0%), Na_2HPO_4 (≥99.0%), NaH_2PO_4 (≥98.0%), NaOH (≥98%), ethanol (≥99.9%), HCl (37%) and 4-(dimethylamino)benzaldehyde (98%) were purchased from Merck (Merck, Germany). Nitrogen (99.995 *V*/V %, Messer Hungarogaz Kft, Hungary) was used for the anaerobization of electrolytes.

2.2. Microbial electrolysis cell setup and biofilm formation

In the first phase of the experiments, triplicate internal cathode chamber MEC reactors (ICC-MEC) were constructed from round bottom glass flasks (anode chamber) and cylindrical plexiglass units (cathode chamber) submerged from the top of the flask (Supplementary material, Fig. A.1a). The anode was graphite fiber brush with a width × length of 3 cm × 3 cm, while the cathode was Ni foam with an apparent surface area of A_C = 8.75 cm^2 (Sigma-Aldrich, USA). The chambers were separated by a Forblue™ Selemion CMVN (AGC, Netherlands) cation exchange membrane (CEM, with a diameter of 2 cm). Anodic biofilm development was initiated by adding 250 mL anolyte solution to the anode chamber, consisting of 50 mM phosphate buffer solution (PBS), 10 *V*/V % anaerobic sludge, modified Wolin's mineral solution, DSMZ 141 vitamin solution and DSMZ 385 selenite-tungstate solution (the exact composition is described elsewhere [19]. During adaptation, the cathode chamber was filled with 14 mL of 50 mM PBS. Acetate was added in consecutive batches (cycles) to the anolyte to set acetate concentration (C_{Ac}) of 5 mM. The electrolytes were replenished between feeding cycles (starting from the 3rd cycle). Anode potential was fixed at 0.2 V versus a SE11 saturated Ag/AgCl reference electrode (Meinsberg Sensortechnik GmbH, Germany) placed near the anode, using chronoamperometry technique and PalmSens3 potentiostat (PalmSens, Netherlands) [20]. Continuous temperature control (37 °C) and electrolyte stirring (150 rpm) was ensured. The catholyte of ICC-MEC was continuously circulated (~ 5 mL min^{-1}) using a peristaltic pump. 16S amplicon metagenomics was carried out on a randomly selected MEC anode sample after the acclimation period. The related methods and protocols are described in detail elsewhere [21].

In order to enhance MEC performance and pH modulation kinetics, optimized cubical 3D-printed MEC (3D-MEC) reactors (Supplementary material, Fig. A.1b) were constructed from polylactic acid filament (3DJake, Austria) using 3D printer (Anycubic Vyper, Anycubic, China). The anode and cathode chambers had working volumes of 160 mL and 40 mL, respectively. A 5 cm × 5 cm CEM (Forblue™ Selemion CMVN, AGC, Netherlands) was used to separate the chambers, and the cathode (0.5 mg cm^{-2} Pt/carbon paper, FuelCellsEtc, USA) had 25 cm^2 apparent surface area. The anode and the reference electrodes, as well as the other operational parameters were identical to the ICC-MEC experiments (the anodes were transferred directly from ICC-MEC reactors).

2.3. Bioelectrochemically assisted pH modulation tests

In the pH modulation tests, either 50 mM PBS (preliminary measurements) or 10-fold diluted synthetic urine was used. Synthetic urine solution was made according to the composition recommended in literature [22]. In the experiments with ICC-MEC reactors, cathode surface area to catholyte volume ratios of A_C/V_C = 0.625, 0.417 and 0.313 cm^2 cm^{-3} were set by changing the catholyte volume (and circulating the catholyte between the cathode chamber and an external container) in order to study its effect on pH increase kinetics and efficiency. In case of 3D-MEC, a fixed A_C/V_C = 0.625 cm^2 cm^3 was applied. The development of catholyte pH (pH_C) along with the actual current density (j) values was monitored during the experiments, mainly to determine the required operation time for ensuring $pH_C \geq 11$, which is the threshold for urease inhibition [23]. After achieving sufficient pH_C, the catholytes' final pH was recorded and the samples were subjected to storage stability tests at 4 °C for 14 days and afterwards, at ambient

temperature for additional 11–14 days. Urea concentration (C_{Urea}) was regularly checked during storage. After the storage phase, 50 unit of urease enzyme (Type IX from *Canavalia ensiformis*, Jack bean, Sigma-Aldrich, USA) was added to the samples (in case of 3D-MEC samples and stored untreated samples as reference point) in order to test urease inhibition efficiency after long-term treatment. One unit corresponds to the enzyme amount which catalysis the hydrolysis of 1.2 mg urea in 5 min at pH = 7 at 21 °C. Enzyme activity at pH = 10 (active urea hydrolysis) was considered as reference point for determining relative urease activity at various pH values.

2.4. Analysis and calculations

Urea concentration was determined using spectrophotometric technique based on 4-(dimethylamino)benzaldehyde reaction [24] and a Hach Lange DR 3900 spectrophotometer (Hach, USA). The composition of the reagent solution is described elsewhere [25]. The 10-fold diluted samples and reagent solution were mixed in 1:1 ratio, and the absorbance (color change to yellow) was recorded at λ = 440 nm after 10 min reaction time. Measurement of pH and electrolyte conductivity (κ) was done using a PCE-228 pH sensor (PCE Instruments, Germany) and a WTW Cond 3110 conductivity meter (Xylem-WTW, USA).

Ion chromatographic measurements were carried out using a Metrohm 882 Compact IC plus – Anion (Metrohm AG, Switzerland). Determination of phosphate ions was carried out using a conductivity detector, and an eluent of 5 mmol L^{-1} Na_2CO_3–5 mmol L^{-1} $NaHCO_3$ at a flow rate of 1 mL min^{-1}, temperature 20 °C and pressure 14.26 MPa. The sample injection volume was 20 μL. Sample dilution was done with MilliQ ultrapure water and the samples were filtered through a 0.22 μm syringe filter before injection (VWR, USA). After injection, the samples first passed through a protective column and then onto the Metrosep A Supp 10–250/4.0 separation column (Metrohm AG, Switzerland).

Polarization behavior of the MEC anodic biofilms was analyzed by recording cyclic voltammograms (CV) in non-turnover mode (after substrate depletion) within a potential window from +0.25 to −0.65 V vs. Ag/AgCl at 1 mV s^{-1} scanning rate, using PalmSens3 potentiostat and the related PSTrace 5.9 data collection software (PalmSens, Netherlands).

Volumetric gas production (Q_G) at the MEC cathode was followed using water displacement method in graduated measuring cylinders, and was calculated relative to the COD provided in grams (m_{COD}). Coulombic efficiency (CE) was determined as the ratio of measured charge (derived from the integral of current – time curves) and maximal theoretical charge based on m_{COD}, as described previously [19]. Hydroxide production efficiency (CE_{OH^-}) was calculated as the measured charge and the theoretically required charge to achieve pH_C = 11. Current density generated in MEC reactors was calculated based on the measured current (I) and the cathode surface area. Absolute (R^P_{abs}) and effective P-recovery (R^P_{eff}) were determined based on the absolute change in phosphate concentration and considering the ratio of phosphate and available bivalent cations as limiting factor for precipitate formation (Eqs. A1 and A2 in the Supplementary material).

3. Results and discussion

3.1. Anode acclimation efficiency and characteristics at poised electrode potential

The proposed concept for urea stabilization and P-recovery is based on the bioelectrochemical activity of electro-active bacteria (EAB) forming a biofilm at the anode surface. Fig. 1 summarizes the fundamental microbiological, electrochemical and chemical processes taking place at the respective compartments of the MEC reactors. In the anode chamber, EAB biofilm formation is promoted by the addition of acetate, which is oxidized by the microbes. The oxidation-derived electrons are transferred to the anode, while protons (and CO_2) are released to the vicinity of the biofilm. Accordingly, depending on the rate of the H^+ diffusion, the pH near the anode decreases compared to the bulk anolyte. Using a CEM, the main cross-membrane transported ions towards the cathode are K^+, Na^+ and H^+ (the latter in orders of magnitude lower extent). At pH values >7, the cathodic reaction is the reduction of water to form H_2 and OH^-, which is driven by the combined energy input of bioelectrochemical activity and external electricity in MEC mode. The presented concept utilizes the effect of the increasing pH value of the catholyte to drive urea stabilization and P-recovery in form of precipitate, both allowed by the sufficiently high catholyte pH (pH > 11, above

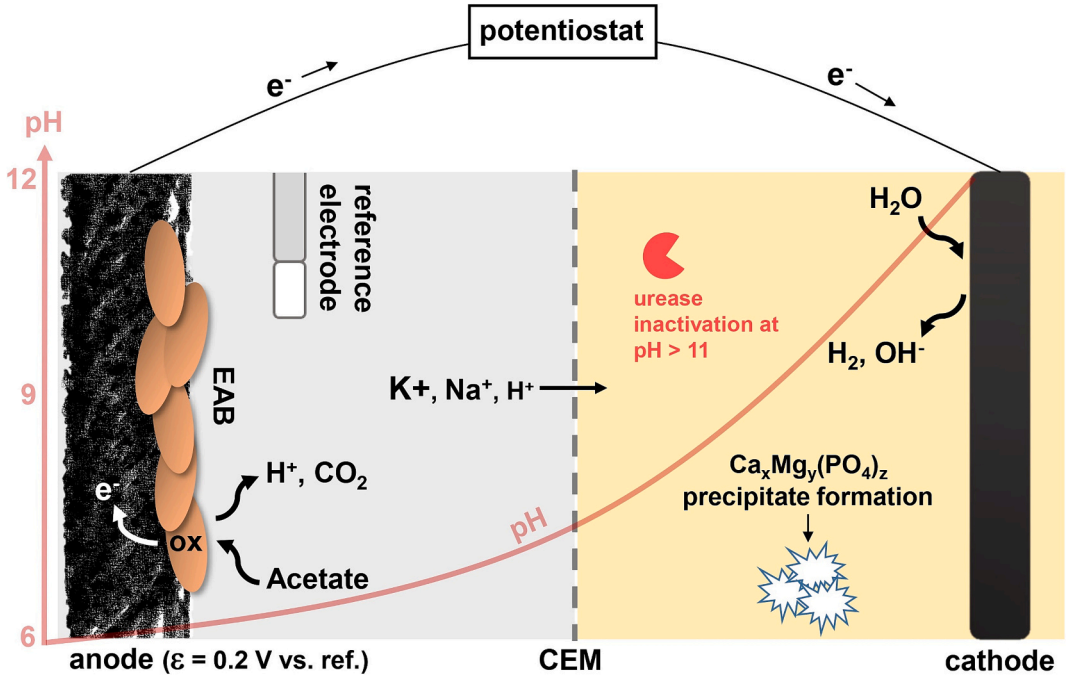

Fig. 1. Schematic of bioelectrochemically assisted pH modulation process.

which urease loses catalytic activity and phosphate forms precipitate with the bivalent cations present). As this scheme indicates, maintaining an EAB biofilm at the anode is key for the process operation. Thus, the first stage of the experiments focused on the anode acclimation.

The formation of the anodic electro-active biofilms was initiated by consecutive batch acetate feedings (cycles) while maintaining an anode potential ($\varepsilon = 0.2$ V vs. Ag/AgCl) widely applied to promote the growth of exoelectrogenic species [20]. As the course of adaptation indicated, bioelectrochemical activity gradually increased over the operation cycles. CE, for instance, was only 7.2 ± 0.35% in the first cycle, and achieved values above 40% from the fifth batch (Fig. 2a). Its peak value in the 8th acetate cycle showed nearly 60% (59.8 ± 10.1%). Thus, a clear development of bioelectrochemical activity could be presumed, indicating successful acclimation of the anode. Similarly to CE, the cathodic gas production also improved during the consecutive cycles. The Q_G initially had a relatively low value of 45.6 ± 23.1 mL g_{COD}^{-1}, which sufficiently increased during operation up to 231.4 ± 31.3 mL g_{COD}^{-1}.

These obtained values are comparable with those communicated previously in literature. For instance, acclimation of graphite felt and brush anodes were investigated in acetate-fed MEC, achieving similar CE of 76 ± 6 and 74 ± 8%, respectively [26]. In another work [27], MECs with various brush anode setups were operated for long term, nearly up to 140 days. The single-brush anode reactors achieved CE = 62–64%, which is also similar to the value recorded in our study at the 8th acetate cycle. As for the hydrogen yields, Q_G = 106–245 mL g_{COD}^{-1} was demonstrated depending on the applied voltage, which also matches well with our results [28]. Nevertheless, higher Q_G values were also reported in literature, where Q_G = 847–1117 mL g_{COD}^{-1} was achieved [29]. These results can be interpreted in the light of the maximal theoretical hydrogen yield of 1419 mL g_{COD}^{-1} [14].

To get insights on the bioelectrochemical behavior of the acclimated anodes, non-turnover CVs were recorded after the completion of the 8th acetate cycle. As it can be seen in Fig. 2b, the fundamental characteristics of CVs were similar for the three MEC anodes, although some inherent differences could be observed regardless of the identical adaptation strategies. At least two redox pairs could be distinguished in the CVs, with formal potentials in the range from −0.1 to −0.25 V vs. Ag/AgCl and from −0.35 to −0.4 V vs. Ag/AgCl, depending on the actual anodes. Also, overlapping peaks were found (for instance in case of ICC-MEC_1 at around −0.2 V vs. Ag/AgCl in the anodic scan). For the most scans, the peak currents were similar (except for example in the cathodic peak of ICC-MEC_2 at ~ −0.57 V vs. Ag/AgCl, which had significantly higher negative peak current compared to other MECs), while the peak potentials showed a shifting tendency among the MECs (Fig. 2b). The (areas of) peak currents are proportional to the concentration of redox species in the system, e.g. the surface coverage of membrane-bound cytochromes on the anode. The observed differences in the peak potential may be explained by a series of MEC parameters, such as subtle biological and electrochemical dissimilarities. For instance, the standard deviance of CE data (Fig. 2a) suggested that although the acclimation parameters were the same in each MECs, the biofilm development took place with different kinetics and efficiency throughout the acetate feeding cycles. Such variations in biofilm maturity (thickness, cell density, cytochrome expression levels, etc.) could lead to peak potential shift through e.g. increased electron transfer resistance or mass transport limitations. In addition, certain (pH, substrate concentration, etc.) gradients can develop near the anode surface, especially in case of brush electrodes, where ensuring homogeneity even in well-mixed reactors faces challenge due to the rather complex structure. Similarly, any change in the reference electrode potential over time could cause peak potential shifts (reference electrodes underwent maintenance regularly). Overall, the CV measurements confirmed that each MECs gained significant bioelectrochemical activity by the end of the acclimation phase, although the developed biofilms were in different maturation stages. To further characterize the biofilm formation, a randomly selected MEC anode was sampled for biofilm microbial consortia analysis, which showed a predominance of *Proteobacteria*, *Firmicutes* and *Desulfobacterota* phyla in the anodic samples, with relative abundances of 50.1, 25.2 and 12.4%, respectively (Fig. A.2a in the Supplementary material). In the level of microbial orders, mainly *Xanthomonadales* (35.3%), *Bacillales* (25.0%) and *Geobacterales* (12.1%) were found on the anode samples, in addition to lower relative abundances of *Burkholderiales* (8.6%), *Bacteroidales* (4.1%) and *Rickettsiales* (3.1%) (Supplementary material, Fig. A.2b). These microbial orders are widely described as common members of anodic (and in some cases, cathodic) biofilms in various bioelectrochemical systems [30–32]. In conclusion, considering that the MEC efficiency, anodic redox activity as well as biofilm microbial consortia parameters indicated sufficient biofilm formation, the adaptation period was considered done, and the MECs could begin to be investigated for targeted pH modulation in different catholytes.

3.2. Bioelectrochemically assisted pH modulation in different catholytes

The main scope of this work is to exploit the pH elevation effect of

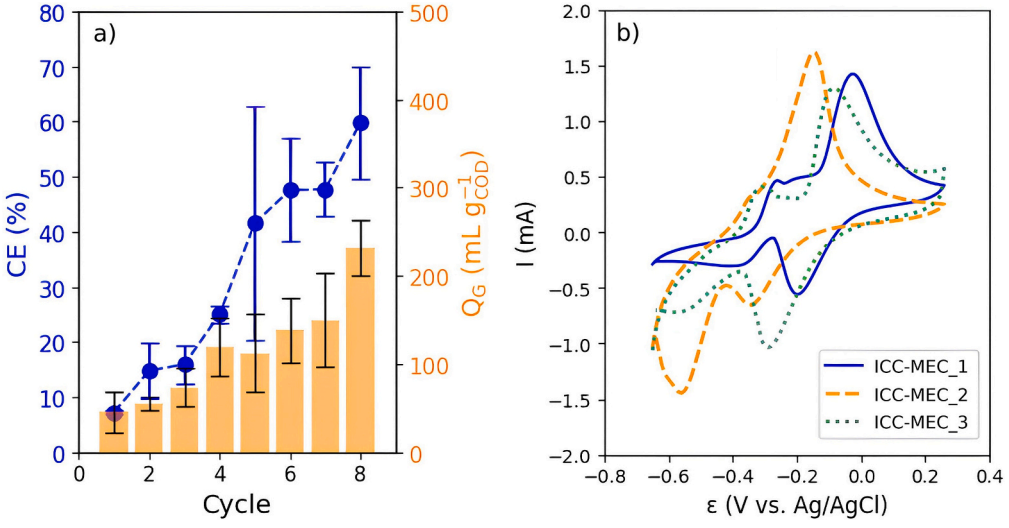

Fig. 2. a) Coulombic efficiency and cathodic gas yield of MECs during the adaptation period (n = 3); b) non-turnover cyclic voltammetry of acclimated ICC-MEC anodes.

the cathodic reaction concurrent to the bioelectrochemical activity for in situ urease enzyme inhibition. According to literature, pH = 11 can be considered as upper limit of urease-catalyzed urea hydrolysis reaction, which was also validated in our work prior to pH modulation experiments [23]. As for the mechanism of urease inhibition caused by the high pH, the specific ionizable groups of the enzyme active sites can be considered. It was shown that especially the protonation states of the Ni—Ni bridging hydroxide (with a $pK_a = 8.67$) and the imidazole groups from histidine residues ($pK_a = 5.34$) of the enzyme should be opposite to maintain catalytic activity, i.e. the bridging hydroxide should be protonated, while the imidazole group should be deprotonated [33,34]. At high pH, both groups are in the same protonation state, which hampers urease activity. In addition, pH was shown to have an effect on the mobility and structural properties of so-called 'mobile flaps' on the urease enzyme, which are flexible structural parts altering between open and closed states and are responsible for substrate binding and transition state stabilization thanks to the geometry of the resulting complex [35,36]. Thus, the negative effect of high (or low) pH on urease activity could be understood as a complex phenomenon consisting of altered protonation states of key groups, as well as structural changes of functional enzyme regions.

To validate the choice of pH = 11 as threshold for urease inhibition, urease activity was recorded at various pH values. Fig. 3 shows the relative activity (i.e. urease activity at different pH values compared to the activity at pH = 10) and the residual urea concentration after 1 h long enzymatic treatment as the function of pH. The results clearly confirmed that the urea hydrolysis is already inhibited at pH = 11, and urease remains inactive in the range of pH = 11–12 as expected. Accordingly, the urea concentration in the pH-treated samples remained constant, while at the reference pH level (pH = 10), >30% of the initial urea was hydrolyzed in one hour. Therefore, pH ≥ 11 was confirmed as a sufficient pH set point in the urea stabilization experiments.

In the following step, the MEC operation was evaluated in terms of the pH modulation efficiency, firstly by using 50 mM PBS as reference catholyte (commonly used in MEC) prior to the synthetic urine test. This approach provides a clear picture on (i) how the cathodic pH developed

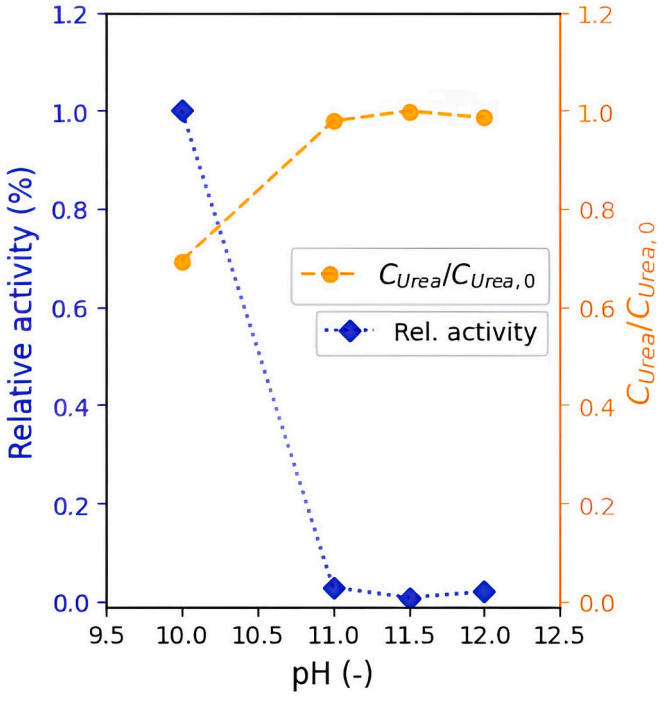

Fig. 3. Relative urease activity and residual urea concentration after enzymatic treatment at different pH values. The relative activity was determined considering urease activity at pH = 10 as reference level.

in the certain acetate feeding cycles through the adaptation period, as well as on (ii) the potentially expectable kinetics and levels of pH build-up in the MEC in the light of the performance. As a result, the final catholyte pH values for PBS at the end of each acetate batches showed an increasing trend during the adaptation period (Fig. 4a). At the first stage (cycle 1–3), the low current generation limited the final pH_C below 11. Nevertheless, further batches and higher currents eventually allowed $pH_C > 11$ from the 4th cycle, and moreover, pH_C as high as 12.8 ± 0.35 could be achieved by the end of the acclimation period (8th cycle).

The results suggest that the constructed MECs could increase the PBS catholyte pH above the desired level. To provide more depth, the process kinetics should be also characterized, since in case of urea stabilization in urine, operation time is preferably minimal, in order to avoid nitrogen loss as a result of persisting urease activity. Therefore, *operando* pH shift profiles were analyzed over three additional acetate feeding cycles, which indicated that – although the batches lasted as long as ~30 h –, the major part of pH elevation (from pH_C = ~ 7 to >11.5) using $A_C/V_C = 0.625$ cm^2 cm^{-3} occurred at the initial stage (first 3 h) of operation in case of PBS (Fig. 4b). In detail, 1 h MEC operation resulted in $pH_C = 9.5 \pm 0.9$, while after 2 h, $pH_C = 10.7 \pm 0.8$ was measured. At 3 h, the pH_C set point was already exceeded ($pH_C = 11.8 \pm 0.2$), and the average trend indicated a required operation time of 127 min to achieve pH_C = 11 (under the present experimental conditions). It is also to note that in some cases, catholyte pH values even above13 were achieved by the end of the batches.

Considering that the preliminary tests with PBS showed promising results for the electrochemical pH modulation, in the next phase, synthetic urine was tested as catholyte. In addition, each MEC reactors operated with different cathode surface area to catholyte volume ratios, namely A_C/V_C = 0.625; 0.417 and 0.313 cm^2 cm^{-3}, in order to investigate their effect on the pH-elevation kinetics and efficiency. Besides, tests were carried out both with C_{Ac} = 5 mM and C_{Ac} = 2.5 mM (sub-optimal substrate dosage), which allowed to assess the role of current density on the process. The lower acetate level resulted in significantly lower current densities (blue line in Fig. 5a-c), and consequently, slower pH elevation in the synthetic urine catholyte compared to C_{Ac} = 5 mM (orange color). In the case of $A_C/V_C = 0.625$ cm^2 cm^{-3} (Fig. 5a), the lower substrate dosage induced an average current density of $j \approx 3.1 \pm 0.1$ A m^{-2}, leading to a steadily increasing pH_C. After 180 min, pH_C was already 11.5, and pH_C = 11 was achieved at ~160 min of operation. With the same A_C/V_C value at C_{Ac} = 5 mM, $j = 4.7 \pm 0.1$ A m^{-2} was achieved, and this was clearly expressed in the time course of pH_C, which passed the set point level at t = 83 min. After this stage, the pH-elevation kinetics was reduced after t > 90 min compared to the earlier stage (Fig. 5a).

As for the ICC-MEC with $A_C/V_C = 0.417$ cm^2 cm^{-3}, Fig. 5b shows that lower C_{Ac} provided only 1.6 ± 0 A m^{-2}, which clearly limited the pH_C build-up. In numbers, at t = 240 min pH_C was only 9.7, and therefore, additional acetate was fed to the ICC-MEC (up to C_{Ac} = 5 mM, indicated by blue arrow in Fig. 5b). This led to rapid j increase up to 4.5 ± 0.2 A m^{-2} for the rest of the operation, and within 60 min (at t = 300 min), pH_C = 11 was achieved. The optimal C_{Ac} = 5 mM acetate addition, however, allowed steady and high current density (j = 4.0 ± 0.1 A m^{-2}) and simultaneously, accelerated pH_C increase. As a result, the set point was reached (pH_C = 11.05) at t = 120 min. In case of $A_C/V_C = 0.313$ cm^2 cm^{-3} (Fig. 5c) the acetate cycle with C_{Ac} = 2.5 mM produced sufficient current density (j = 3.4 ± 0.1 A m^{-2}), although it gradually fell under 3 A m^{-2} after 300 min of operation. Meanwhile, the pH_C set point could be realized only at t = 390 min. By ensuring higher j (~ 4.2 ± 0.1 A m^{-2}) at C_{Ac} = 5 mM, rapid and steady pH modulation could be done in the synthetic urine, and the level of pH_C = 11 could be observed at t ≈ 135 min.

Considering the efficiency of the process, CE_{OH^-} values (taken into account only for the tests at C_{Ac} = 5 mM) indicated that the MEC setup with A_C/V_C ratio of 0.625 cm^2 cm^{-3} proved to be the most effective, reaching CE_{OH^-} = 10.0% during pH modulation to 11. This means that

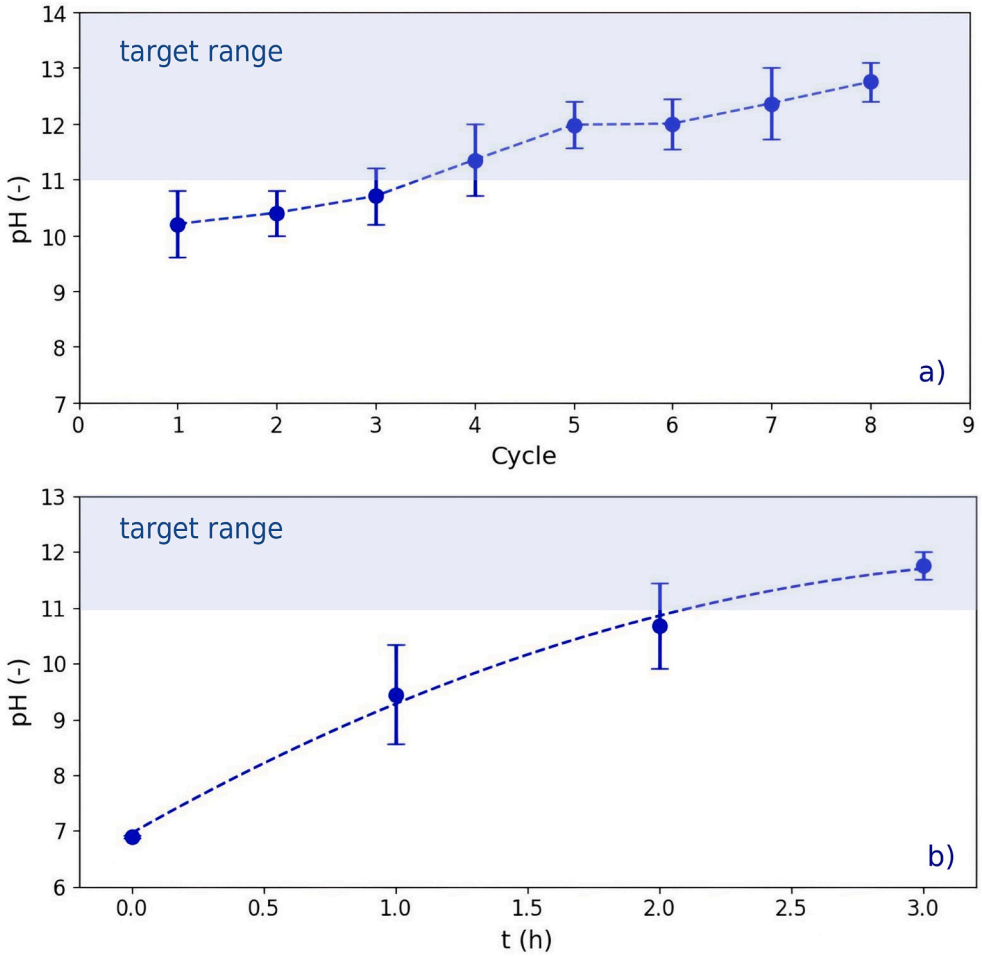

Fig. 4. Final PBS catholyte pH values of the acclimation cycles (a), and pH build-up at $j = 4.2 \pm 0.2$ A m^{-2} in the 50 mM PBS catholyte (b) over time in the ICC-MEC (n = 3). The target range of pH > 11 for sufficient urease inhibition is highlighted with light blue background color. (For interpretation of the references to color in this figure legend, the reader is referred to the web version of this article.)

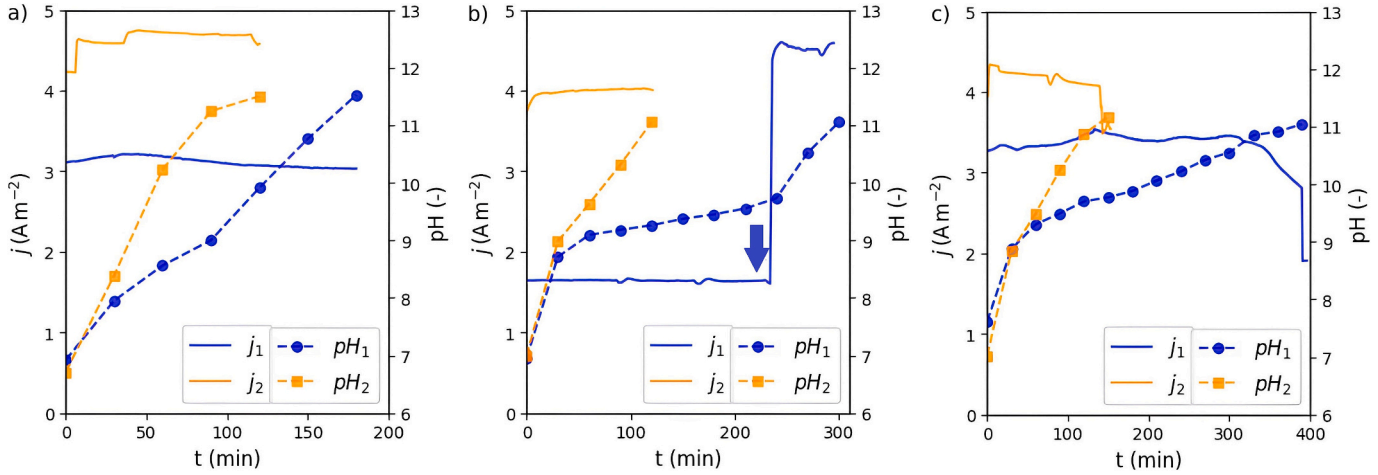

Fig. 5. Bioelectrochemical pH modulation tests with synthetic urine in ICC-MEC at A_C/V_C ratios of a) 0.625; b) 0.417 and c) 0.313 cm^2 cm^{-3}. Continuous lines show the actual current density profile during pH elevation process. The experiments with each A_C/V_C ratios were carried out at C_{Ac} = 5 mM (orange) and C_{Ac} = 2.5 mM (blue) concentration. The arrow on graph b) indicates additional acetate input (compensating low current generation). (For interpretation of the references to color in this figure legend, the reader is referred to the web version of this article.)

increasing the OH^- concentration (in this case to a level of 1 mM) in the synthetic urine catholyte is a rather limited process at the given current density range. Moreover, a decreasing trend could be observed in line with the reduction of A_C/V_C ratio. In the case of A_C/V_C = 0.417 cm^2 cm^{-3}, CE_{OH^-} was only 8.1%. Furthermore, CE_{OH^-} was as low as 6.9% in case of A_C/V_C = 0.313 cm^2 cm^{-3}. This accounts for nearly 20% drop in

CE_{OH^-} as a response to the 50% reduction in A_C/V_C.

Based on the experimental results obtained with the ICC-MEC, and taking the relatively low CE_{OH^-} values into consideration, more practical and optimized reactors were constructed based on 3D-printing technology (3D-MEC). These MEC reactors operated with a fixed A_C/V_C ratio of 0.625 cm^2 cm^{-3}, adapted from the ICC-MEC setup with the best pH increase kinetics. The already obtained and used bioelectrochemically active anodes were transferred to the 3D-MEC reactors, and after confirming undisrupted biofilm activity, pH modulation experiments were initiated with synthetic urine and C_{Ac} = 5 mM. The three 3D-MEC reactors operated in parallel were denoted as 3D-MEC_1, 3D-MEC_2 and 3D-MEC_3. As it could be observed from the current generation profiles, two of the three 3D-MEC produced higher j compared to the previously presented ICC-MEC reactors (Fig. 6). In fact, 3D-MEC_2 and 3D-MEC_3 showed average current densities of 5.4 ± 0.2 and 4.6 ± 0.2 A m^{-2} throughout the experiments, which was accompanied by a rapid pH_C increase. The pH set point could be achieved at t = 55 and 62 min in case of 3D-MEC_2 and 3D-MEC_3, respectively, and thus, the pH modulation process could be done in 33.7 and 25.3% lower operation time compared to the results of ICC-MEC with A_C/V_C = 0.625 cm^2 cm^{-3}.

At the same time, the reactor labelled as 3D-MEC_1 showed a rather limited current generation capacity with as low as j = 1.43 ± 0.1 A m^{-2} average current density, and thus, a significantly slower increase of pH in the catholyte (Fig. 6). Overall, >1000 min operation time was required to ensure pH_C = 11, which is remarkably higher than in any other cases during the experiments. Nevertheless, the evaluation of CE_{OH^-} for this set of pH modulation experiments revealed some valuable aspects. Firstly, in case of the well-performing 3D-MEC_2 and 3D-MEC_3 reactors, CE_{OH^-} = 24.6 and 25.9% could be achieved, which is a major improvement in the light of the ICC-MEC efficiency. Secondly, the further comparison of results with ICC-MEC confirmed that there is significant room for performance improvement through optimizing the bioelectrochemical reactor design. The 3D-MEC offers a more practical electrolyte volume ratio of the anolyte/catholyte (V_A:V_C = 4:1), and the ion transfer proceeds through a higher CEM surface area, which further promotes the overall process efficiency. For comparison purposes with alternative electrochemical OH^- generation and pH modulation techniques, e.g. water softening could be considered. It was shown in literature that in case of electrochemical treatment of unbuffered deionized water with 5 mM NaCl content (at current density of 5 A m^{-2}) to a final OH^- level of 1.4 mM required 32 min at $CE_{\overline{OH}}$ = 14% [37]. Also, applying j = 15 A m^{-2} for the same catholyte, but to produce final OH^- concentration of 2.8 mM, 13 min was needed, although $CE_{\overline{OH}}$ was only 24%. Thus, the data obtained with MEC indicate that the efficiency of the bioelectrochemical treatment is in good agreement with more energy-demanding electrochemical techniques.

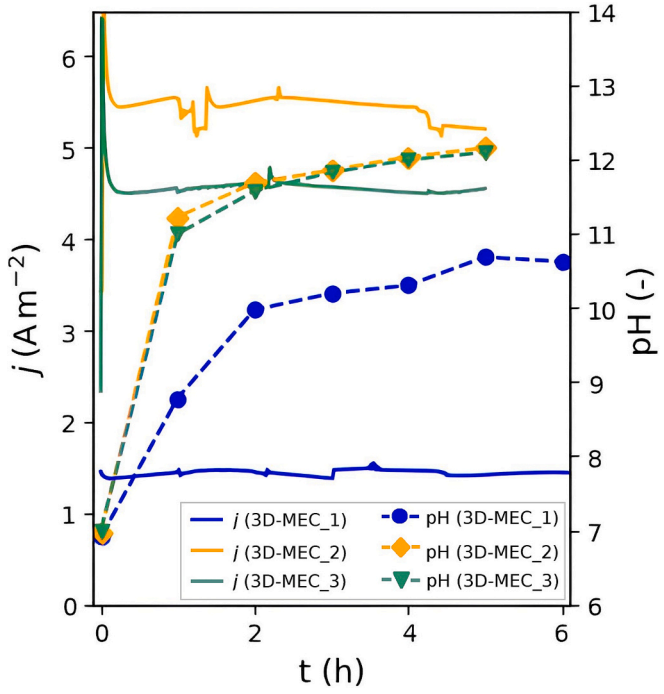

Fig. 6. Bioelectrochemical pH modulation tests with synthetic urine in 3D-MEC at A_C/V_C = 0.625 cm^2 cm^{-3}. Continuous lines show the actual current density at C_{Ac} = 5mM during pH increase (dashed lines).

3.3. Urea stabilization efficiency and phosphate recovery

The efficiency of the novel bioelectrochemically assisted pH modulation method presented in this work was further tested in terms of the stability of pH-treated synthetic urine. As the main objective was to ensure stable urea content by inhibiting enzymatic urea hydrolysis via increased solution pH, monitoring of C_{Urea} (and pH) was carried out for at least 25 d in the stored samples. Fig. 7a shows the changes in C_{Urea} (compared to the initial value) for 3–3 stabilized synthetic urine samples derived from the experiments with ICC-MEC and 3D-MEC, respectively. It could be observed that urea stabilization was successful in case of both MEC setups, and accordingly, urea concentration did not decrease significantly during storage regardless of the temperature. In case of ICC-MEC, C_{Urea} of the samples was slightly more consistent compared to 3D-MEC samples, and 99 ± 4% of the initial urea concentration was measured on the 25th day. As for the 3D-MEC – although the SD among the samples was higher – an average of 93 ± 8% of the initial C_{Urea} was recorded after 28 d (Fig. 7a).

Prior to the storing tests, urea concentrations referring to the endpoint of the pH modulation processes were recorded. As for the ICC-MEC, it appeared that lower A_C/V_C ratios (i.e. longer duration of reaching the pH threshold) corresponded with lower C_{Urea} in the treated samples. In fact, C_{Urea} = 1.47, 1.35 and 1.10 g L^{-1} was determined at the end of the pH modulation process for A_C/V_C = 0.625, 0.417 and 0.313 cm^2 cm^{-3}, respectively. The samples stabilized in 3D-MEC_2 and 3D-MEC_3 showed final C_{Urea} of 1.11 and 1.06 g L^{-1} (at j = 5.4 ± 0.1 and 4.6 ± 0.1 A m^{-2} current densities), while in the case of 3D-MEC_1 (where j was only 1.43 ± 0.4 A m^{-2} and pH_C = 11 was achieved only after 1000 min of operation) C_{Urea} = 0.66 g L^{-1} could be obtained. These data led to new insights on the process efficiency details: it turns out that longer operation time is accompanied by lower urea concentration in the stabilized synthetic urine samples in both MEC setups. This phenomenon can be a direct effect of mainly (i) residual urease activity expressing its effect parallel with the pH modulation process, (ii) partial (electro) chemical degradation of urea during the treatment, or (iii) diffusive loss of urea due to cross-membrane transport. As for the simultaneously occurring enzymatic hydrolysis of urea, it is assumed to be the most plausible explanation, since microbial contamination with urease-positive species is likely present in the cathode compartment of MEC reactors, even though the main processes here are non-biological. Besides, non-enzymatic urea hydrolysis could take place according to Eq. 2 in alkaline media [38].

$$CO(NH_2)_2 + 2OH^- \rightarrow 2NH_3 + CO_3^{2-} \quad (2)$$

This irreversible reaction is hypothesized to proceed via the attack of the carbonyl carbon of urea by the OH^- [39]. The effect of parameters such as pH and temperature on the rate of the reaction is widely described [23,40,41], and according to those, the half-life of urea (even at pH = 12–13) lies in the range of 8–10 d at 66 °C, and accordingly, even higher at mesophilic temperatures (37 °C) representing the MEC conditions. Since the pH modulation process in most cases is completed in a few hours, such slow non-enzymatic hydrolysis would not likely take place in a relevant extent in our experiments. It is to mention, however, that in case of higher pH (~ 14) values, half-life of urea

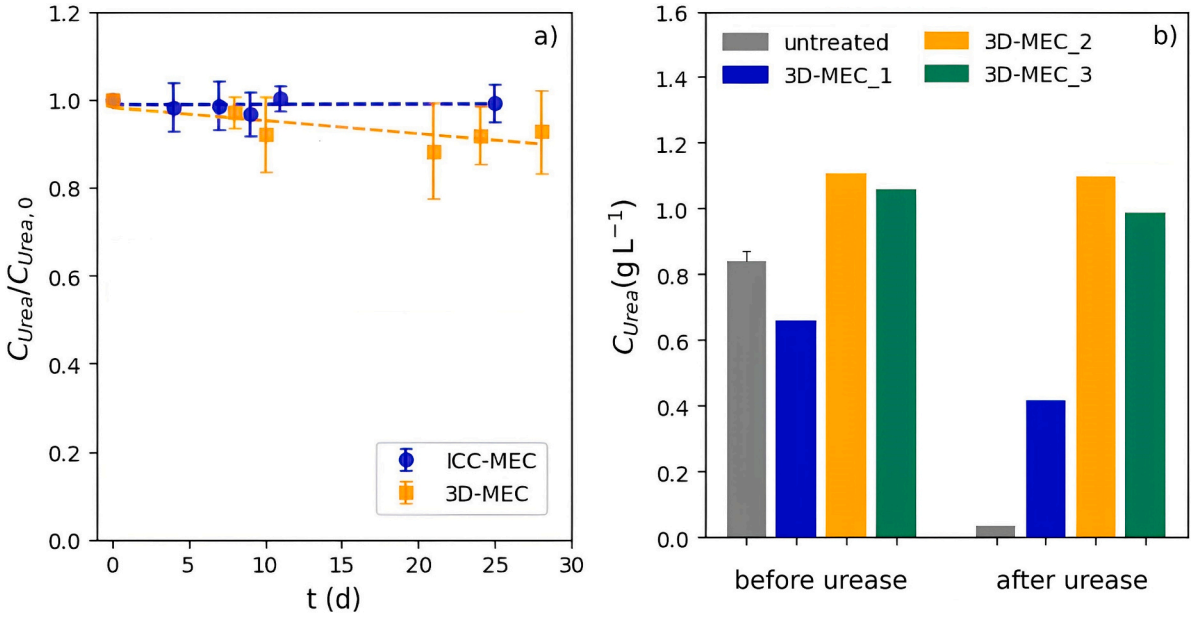

Fig. 7. Stability results (change of urea concentration compared to its initial value) of pH modulated samples (n = 3) during storage at 4 °C (14 d) and ambient (additional 11–14 d) temperature (a), and the enzymatic hydrolysis assays of untreated and pH modulated samples after storage tests (b).

reduces to hours [23]. In the vicinity of the MEC cathode, local pH gradients are naturally expected. Assuming a theoretical calculation approach, and a diffusion layer thickness of e.g. 100 μm at the cathode (relevant for porous cathodes in stirred systems), and the average current density range of the MEC reactors in this work, Faraday's law would suggest that local hydroxide concentrations near the cathode may reach pH ≈ 13.7 at $CE_{OH^-} = 100\%$. In such case, the reaction rate constant (k) for non-enzymatic urea hydrolysis (calculating with a half-life of $t_{1/2}$ = 5 h and $CE_{OH^-} = 100\%$) gives $k \approx 3.85 \times 10^{-5}\ s^{-1}$. Using a simple first-order kinetics ($C_{Urea} = C_{Urea,0} \times \exp.(-k \times t)$), this reaction rate constant would result in a concentration change of $\Delta C_{Urea} \approx 0.2\ g\ L^{-1}$ in one hour, i.e. 13% decrease of C_{Urea}. Nevertheless, in the light of the obtained CE_{OH^-} values of ~6.9–25.9% (and the mild reaction temperature), a significantly lower pH could be expected at the surface of the electrode, and thus, non-enzymatic base-catalyzed hydrolysis of urea could be considered as a rather negligible factor in the experiments, presumably accounting for only a few percent urea loss at most. The aspect of the potential cross-membrane urea loss is discussed in detail in Section 3.4.

The samples (from the 3D-MEC experiments together with untreated samples) were subjected to urease treatment after the storing stability tests to investigate the enzyme inhibition capacity. The results presented in Fig. 7b clearly demonstrated the good efficiency of urease inhibition (i.e. urea stabilization) mainly for the pH modulated samples at sufficient j. As for the untreated synthetic urine, the 1 h long enzymatic reaction led to nearly complete (~95.4%) removal of urea (at initial pH of 7.4). In the case of the 3D-MEC_1, (due to the low j and consequently the long pH modulation time) the already low C_{Urea} was further reduced after the urease addition, namely by 37.0% (Fig. 7b). This was explained by the shift in pH for this sample during the 30-day long storage. It was seen that although the catholyte pH could achieve the threshold value of 11 after long-drawn operation at low j in 3D-MEC_1, the solution pH gradually decreased back to pH = 8.4, and in addition, a slight cloudiness was observed in the solution, indicating overall that such long treatment time (>1000 min) did not result in sufficient stability, and that – although apparently slower – enzymatic hydrolysis took place after urease addition. Nevertheless, in the case of 3D-MEC_2 and 3D-MEC_3 – for which the pH modulation was rapid thanks to the high j – efficient urease inhibition was demonstrated. In these samples, the measured alteration in C_{Urea} (0.9–4.1%) remained below the natural error of the measurement. This was in good agreement with their pH determined before urease addition, which in both cases were > 11.5. To broaden the evaluation, the results were compared with literature data on urea stabilization applying various techniques (e.g., chemical, electrochemical) (Table A1, Supplementary Material).

The recovery of phosphorus is another significant aspect of urine treatment and utilization techniques, since it could offer an inexhaustible renewable source of P. Electrochemically induced precipitation of phosphate not only allows collecting P and N in separate phases during the process, but also reduces clogging issues in urine collection systems thanks to the removal of bivalent ions (calcium and magnesium) from urine. This approach was previously addressed in literature with abiotic electrochemical systems, and to the best of our knowledge, this is the first time that it is studied in MEC. Accordingly, P-recovery was evaluated in addition to urea stabilization studies. In our experiments, above pH ≈ 10.6–10.8, precipitates were gradually formed in the catholyte. Preliminary studies showed in transmission electron microscopy assays that this substance was amorphous calcium magnesium phosphate (ACMP) [25]. The recovery of phosphorus through the precipitation of phosphate is limited by the amount of Ca^{2+} and Mg^{2+} ions. In the synthetic urea, the ratio of the amounts of bivalent ions to phosphate is roughly 1:4. Moreover, the ratio of Ca:Mg:P in the precipitate was 0.93:0.35:1. Thus, without further addition of Ca^{2+}/Mg^{2+}, slightly more than 20% maximal P-recovery can be achieved due to the depletion of bivalent ions. In our experiments, residual phosphate concentrations in 3D-MEC_2 and 3D-MEC_3 samples revealed absolute P-recovery of R^P_{abs} = 19.4% and 13.9% (equal to effective P-recovery of R^P_{eff} = 96.5% and 66.7%, with respect to the maximal achievable P-recovery limited by the amount of bivalent ions), respectively (no data for 3D-MEC_1). These data suggest that phosphate precipitation, although not up to its theoretical maximum, but takes place with a considerable extent during the pH modulation under the current experimental conditions and targeted pH threshold. It is likely that precipitate formation would benefit from longer operation times and higher obtained pH values in the synthetic urine, which appears like a potential trade-off between efficient stabilization of urea and P-recovery. Nevertheless, this insight highlights another optimization aspect, and accordingly, phosphate precipitation kinetics from urine should be also addressed in further research. The results are comparable with P-recovery efficiencies achieved with other methods and substrates. For instance, the electrochemical P-recovery from cheese wastewater resulted in nearly 90% using I = 300 mA and 48

h operation time [42]. Similarly, other techniques, such as by using sacrificial Mg electrodes were shown to be effective to recover phosphate mainly as Mg-phosphate with efficiencies of 87–95% [43]. Flow-electrode capacitive deionization was also applied for selective urea and phosphate (H_3PO_4) recovery, exceeding 90% with >90% purity [44]. An electrochemical nutrient recovery cell was investigated for the treatment of digested anaerobic sludge, which, besides high normalized energy consumption, allowed 42–90.3% P-recovery in water electrolysis mode [45]. Moreover, at lower current density application (0.04 A m^{-2}), 27% of P was recovered after 4 days of operation [46] (in comparison, our tests were even as short as 1 h). The findings indicate that bioelectrochemically assisted pH modulation could demonstrate comparable performance to that of other reported methods. It is also to mention that the more complex matrix of real urine might alter the MEC and process performance during treatment, mostly due to factors such as the presence of (i) ammoniacal N, (ii) various organic compounds or (iii) co-precipitating components (carbonate, sulphate). Besides inducing potential competing precipitate formation, electrode fouling, reduced selectivity and additional buffering capacity could be anticipated. Future research should evaluate these aspects for the deeper understanding of fundamental differences between treatment performance with model and real systems.

3.4. Assessment of mass transport and energetic losses

As mentioned in Section 3.3.e, longer residence time of urea in the MEC reactors resulted in slightly lower C_{Urea} in the stabilized solutions compared to its initial concentration. In addition to residual urease activity in the MEC and the potential electrochemical breakdown of some parts of urea, non-ionic membrane crossover can also be hypothesized. To address this phenomenon, a diffusion cell was assembled with two chambers separated by the same CEM as in case of the MEC experiments. A cross-membrane urea concentration gradient was ensured by setting $C_{Urea} = 1.5$ g L^{-1} in one chamber, while the other contained distilled water. After regular sampling of the downstream phase (no urea content initially), urea transport could be quantified. Accordingly, a linear, gradually increasing urea concentration was observed in the 24 h long measurement. Nevertheless, the transported amounts were rather low. In the first 2 h the recorded urea level in the downstream phase was only 4 mg L^{-1}, while it increased to slightly more than 35 mg L^{-1} after 24 h. Mass transport coefficient of urea (k_{Urea}) was also determined based on the diffusion cell measurements, according to Eq. 3:

$$k_{Urea} = \frac{V}{A_M \times t} ln\left(\frac{C_{Urea,0}}{C_{Urea,0} - C_{Urea,t}}\right) \quad (3)$$

where V and A_M are the solution volume and the surface area of the membrane, while $C_{Urea,0}$ and $C_{Urea,t}$ are the urea concentrations at the beginning of the experiments and at time t. The results showed low urea mass transfer with $k_{Urea} = 1.37 \times 10^{-5}$ cm s^{-1}. Considering the thickness of the CEM ($\Delta x \approx 100$ μm), the diffusion coefficient of urea can be calculated as the product of $k_{Urea} \times \Delta x = D_{Urea} = 1.37 \times 10^{-7}$ cm^2 s^{-1}. The diffusive flux of urea (J_{Urea}) is therefore given as $J_{Urea} = D_{Urea} \times \Delta C_{Urea}/\Delta x = 2.06 \times 10^{-8}$ g cm^{-2} s^{-1}. In the light of this, in the 3D-MEC, where the membrane area is 25 cm^2, a 1-h long treatment would account for the cross-over of <2 mg urea under the given experimental conditions. This value corresponds to <1% loss of urea per hour, which can confidently be considered negligible under the presented experimental conditions. In addition, taking both cross-membrane urea transport and non-enzymatic urea hydrolysis (as discussed in Section 3.3) into account, these processes could only explain less than 5% of the urea loss during process (in case of 3D-MEC, and even lower for ICC-MEC where A_M is significantly smaller), which further supports the assumption that there could be residual urease activity in the MEC cathodic environment during the experiments.

Besides mass transport limitations related directly to urea, MEC performance suffers losses also due to the compositional changes of the electrolyte during operation. Two major factors often being considered in this aspect are the overpotentials of (i) pH imbalance and (ii) ion transfer phenomena. The pH imbalance, or as often referred to, pH splitting occurs naturally in most cases of bioelectrochemical systems, including MEC. On the one hand, the anodic (mainly biological) oxidation processes often result in acidification in the biofilm, due to the accumulation of the released protons at the electrode surface. To maintain electroneutrality, the transfer of H^+ is not energetically favorable for the most part of the reactors' operation, since – in case of using CEM – the cross-over of other ions, such as K^+ and Na^+ dominate the charge transfer according to their significantly higher concentrations compared to protons [15,47]. On the other hand, the cathode reactions in e.g. MFC and MEC results in the generation of OH^- ions. In general, and especially in terms of overpotentials, the increasing pH deteriorates the system performance, even though in the present work, this effect was aimed to be exploited for urea stabilization. In theory, a loss of 59 mV ($E_{\Delta pH}$) is attributed to each unit of pH difference between the anode and cathode electrodes [48]. At the same time, the electrolyte conductivities / resistances associated with the composition of ionic species lead to ionic overpotential (E_{ionic}), which mostly depends on the geometry and the ionic current flow in the bioelectrochemical reactor. Based on the experimental results, $E_{\Delta pH}$ and E_{ionic} were determined according to Eq. 4 and Eq. 5 [49,50]:

$$E_{\Delta pH} = \frac{R \times T}{F} ln\left(10^{(pH_C - pH_A)}\right) \quad (4)$$

$$E_{ionic} = j\left(\frac{l_A}{\kappa_A} + \frac{l_C}{\kappa_C}\right) \quad (5)$$

where l_A and l_C are the distances of the membrane and anode / cathode, while κ_A and κ_C are the measured conductivities in the anolyte and catholyte, respectively. The related data are shown for the 3D-MEC reactors, where in addition to the high performance, the geometry was also more regular compared to ICC-MEC. In addition to the final pH_C values of 3D-MEC_1, 3D-MEC_2 and 3D-MEC_3 at the end of the MEC treatment (namely, $pH_C = 11.3$, 12.1 and 12.1), the final anolyte pH values were $pH_A = 5.9$, 6.2 and 6.4, respectively. As it can be seen in Table 1, the pH-related overpotential was the highest in case of 3D-MEC_2, where the largest pH splitting occurred. The $E_{\Delta pH}$ was only 5.5 and 10.5% lower for 3D-MEC_3 and 3D-MEC_1.

The ionic overpotentials followed the trend observed for $E_{\Delta pH}$, i.e. the value of E_{ionic} was proportional to the current generation of the MEC reactors. At the same time, the ionic losses were less than third of the pH-related overpotentials. This phenomenon was also observed previously in MEC studies with non-PBS catholytes, such as NaCl [29]. Thus, we can conclude that there is a reasonable trade-off between the enhanced current density (and therefore, enhanced pH build-up kinetics) and the occurring losses in the MEC using synthetic urine as catholyte, and moreover, these losses are predominantly determined by the level of pH splitting.

Considering the specific electric energy consumption (eec) of the process, the applied voltage (U, conventional MEC mode), current, operational time and the volume of the treated urine (V_U) should be considered according to Eq. 6.

Table 1
– Differences of pH and conductivity between the anolyte and catholyte, and the values of pH- and ionic overpotentials.

Reactor ID	ΔpH (–)	Δκ (mS cm^{-1})	$E_{\Delta pH}$ (mV)	E_{ionic} (mV)
3D-MEC_1	5.4	0.96	322.6	29.6
3D-MEC_2	5.9	0.12	360.6	109.4
3D-MEC_3	5.7	0.44	340.7	99.8

$$eec = \frac{U \times I \times t}{V_U} \quad (6)$$

In our case, the exact cell voltage is unknown as the cathode potential was not monitored. Also, cathode potential would show a shift as the catholyte pH increases during the stabilization process. Nevertheless, in MEC studies, theoretically U = 0.2 V could drive the cathodic reaction together with the bioelectric contribution. However, due to the various losses, real systems require in average 0.8 V of external voltage. Considering the more sufficient case of 3D-MEC reactors, the average current was ~12.5 mA, the reaction time till reaching pH = 11 was ~1 h, and the catholyte volume was 25 cm^3. Combining these values with the realistic voltage requirement of 0.8 V, an eec = 250 Wh m^{-3} could be estimated (or in absolute energy unit, a MEC with the parameters of our study would require eec ≈ 10 mWh). This value is significantly lower than those obtained for pure electrochemical stabilization of the same synthetic urine stream (up to 1.2 kWh m^{-3}) [25]. In comparison, eec can be given specified to kg of P recovered (eec_P). In this term, the present data showed comparable, and in several cases, even lower eec_P values, namely 15.7–21.9 kWh kg^{-1}-P, compared to existing electrochemical methods in literature for waste-based P-recovery, ranging between 23.9 and 229 kWh kg^{-1}-P [51–53].

4. Conclusions

This work investigates the feasibility of a novel bioelectrochemically assisted urea stabilization method in synthetic urine via in situ cathodic pH modulation in MECs. The effect of cathode surface area to catholyte volume ratio, and current density on the pH modulation kinetics was evaluated. Optimized 3D-printed MEC reactor allowed enhanced pH increase efficiency and reduced operational time for urea stabilization compared to internal cathode chamber design. pH modulated synthetic urine samples remained stable during nearly 1 month of storage, and afterwards, showed remarkable urease inhibition efficiency during enzymatic treatment. In addition to the sufficient stabilization of urea, absolute and effective P-recoveries up to 19.4% and 96.5% were achieved. To provide more insight on the process, mass transport-related and energetic losses due to pH splitting and ion migration were evaluated. Future research should focus on adopting the present findings to the treatment of real urine in MEC, as well as to investigate the scale-up of the technology.

CRediT authorship contribution statement

Kristóf Bence Nagy: Writing – original draft, Investigation, Formal analysis, Data curation, Conceptualization. **Mónika Meiczinger:** Writing – original draft, Investigation, Formal analysis. **Boglárka Bocska:** Visualization, Investigation, Formal analysis, Data curation. **Nándor Nemestóthy:** Resources, Methodology, Funding acquisition. **László Koók:** Writing – original draft, Visualization, Supervision, Project administration, Methodology, Funding acquisition, Formal analysis, Conceptualization.

Declaration of competing interest

The authors declare that they have no known competing financial interests or personal relationships that could have appeared to influence the work reported in this paper.

Acknowledgements

L.K. was supported by the János Bolyai Research Scholarship of the Hungarian Academy of Sciences. This research was funded by the National Multidisciplinary Laboratory for Climate Change (RRF-2.3.1-21-2022-00014) project by the government of Hungary.

Appendix A. Supplementary data

Supplementary data to this article can be found online at https://doi.org/10.1016/j.cej.2025.165154.

Data availability

Data will be made available on request.

References

[1] P. Ledezma, P. Kuntke, C.J.N. Buisman, J. Keller, S. Freguia, Source-separated urine opens golden opportunities for microbial electrochemical technologies, Trends Biotechnol. 33 (2015) 214–220, https://doi.org/10.1016/j.tibtech.2015.01.007.
[2] K.M. Udert, T.A. Larsen, W. Gujer, Fate of major compounds in source-separated urine, Water Sci. Technol. 54 (2006) 413–420, https://doi.org/10.2166/wst.2006.921.
[3] H.L.T. Mobley, R.P. Hausinger, Microbial ureases: significance, regulation, and molecular characterization, Microbiol. Rev. 53 (1989) 85–108, https://doi.org/10.1128/mmbr.53.1.85-108.1989.
[4] T.A. Larsen, K.M. Udert, J. Lienert, Source separation and decentralization for wastewater management, IWA Publishing (2015), https://doi.org/10.2166/9781780401072.
[5] T.A. Larsen, M.E. Riechmann, K.M., Udert, state of the art of urine treatment technologies: a critical review, Water Res. X 13 (2021) 100114, https://doi.org/10.1016/j.wroa.2021.100114.
[6] Y. Liu, L.F. He, Y.Y. Deng, Q. Zhang, G.M. Jiang, H. Liu, Recent progress on the recovery of valuable resources from source-separated urine on-site using electrochemical technologies: a review, Chem. Eng. J. 442 (2022) 136200, https://doi.org/10.1016/j.cej.2022.136200.
[7] P.H. Arve, S.C. Popat, Stabilization of urea for recovery from source-separated urine using electrochemically synthesized hydrogen peroxide, ACS ES&T Eng. 1 (2021) 1642–1648, https://doi.org/10.1021/acsestengg.1c00194.
[8] L. Xu, R. Ding, Y. Mao, S. Peng, Z. Li, Y. Zong, D. Wu, Selective recovery of phosphorus and urea from fresh human urine using a liquid membrane chamber integrated flow-electrode electrochemical system, Water Res. 202 (2021) 117423, https://doi.org/10.1016/j.watres.2021.117423.
[9] J. De Paepe, L. De Pryck, A.R.D. Verliefde, K. Rabaey, P. Clauwaert, Electrochemically induced precipitation enables fresh urine stabilization and facilitates source separation, Environ. Sci. Technol. 54 (2020) 3618–3627, https://doi.org/10.1021/acs.est.9b06804.
[10] M.K. Perera, J.D. Englehardt, Simultaneous nitrogen and phosphorus recovery from municipal wastewater by electrochemical pH modulation, Sep. Purif. Technol. 250 (2020) 117166, https://doi.org/10.1016/j.seppur.2020.117166.
[11] K. Govindan, S.J. Im, V. Muthuraj, A. Jang, Electrochemical recovery of H2 and nutrients (N, P) from synthetic source separate urine water, Chemosphere 269 (2021) 129361, https://doi.org/10.1016/j.chemosphere.2020.129361.
[12] M.K. Perera, J.D. Englehardt, J.L. Cohn, E.A. Dauer, D. Shukla, Electrohydromodulation for phosphate recovery from wastewater, Sep. Purif. Technol. 247 (2020) 116909, https://doi.org/10.1016/j.seppur.2020.116909.
[13] H. Kim, H. Park, K. Kim, C. Lee, Electrochemical recovery of nutrients from human urine coupled with biogas upgrading, Bioresour. Technol. 394 (2024) 130298, https://doi.org/10.1016/j.biortech.2023.130298.
[14] B.E. Logan, D. Call, S. Cheng, H.V.M. Hamelers, T.H.J.A. Sleutels, A.W. Jeremiasse, R.A. Rozendal, Microbial electrolysis cells for high yield hydrogen gas production from organic matter, Environ. Sci. Technol. 42 (2008) 8630–8640, https://doi.org/10.1021/es801553z.
[15] T.H.J.A. Sleutels, A. ter Heijne, P. Kuntke, C.J.N. Buisman, H.V.M. Hamelers, Membrane selectivity determines energetic losses for ion transport in bioelectrochemical systems, ChemistrySelect 2 (2017) 3462–3470, https://doi.org/10.1002/slct.201700064.
[16] M. Xu, M.F.-A. Cobo, D. Zeng, Y. Zhang, Leveraging 3D printing in microbial electrochemistry research: current progress and future opportunities, Front. Environ. Sci. Eng. 19 (2025) 1, https://doi.org/10.1007/s11783-025-1921-y.
[17] A. Kim, A. Simson, Rapid optimization of 3D printed sediment microbial fuel cells, international journal of energy and environmental, Engineering 14 (2023) 243–255, https://doi.org/10.1007/s40095-022-00524-2.
[18] C.-C. Chang, C.-W. Yeh, C.-P. Yu, Scaling up 3D-printed urine microbial fuel cells with the membrane electrode assembly, J. Power Sources 582 (2023) 233549, https://doi.org/10.1016/j.jpowsour.2023.233549.
[19] L. Koók, A. Hajgató, K.B. Nagy, K. Bélafi-Bakó, N. Nemestóthy, Comparative assessment of microbial desalination cells and microbial electrolysis desalination cells: towards improved salt removal kinetics and efficiency, Desalination 598 (2025) 118406, https://doi.org/10.1016/j.desal.2024.118406.
[20] C. Gimkiewicz, F. Harnisch, Waste water derived electroactive microbial biofilms: growth, maintenance, and basic characterization, J. Vis. Exp. 82 (2013) 50800, https://doi.org/10.3791/50800.
[21] S. Szakács, L. Koók, N. Nemestóthy, K. Bélafi-Bakó, P. Bakonyi, Studying microbial fuel cells equipped with heterogeneous ion exchange membranes: electrochemical performance and microbial community assessment of anodic and membrane-surface biofilms, Bioresour. Technol. 360 (2022) 127628, https://doi.org/10.1016/j.biortech.2022.127628.

[22] N. Sarigul, F. Korkmaz, İ. Kurultak, A new artificial urine protocol to better imitate human urine, Sci. Rep. 9 (2019) 20159, https://doi.org/10.1038/s41598-019-56693-4.
[23] D.G. Randall, M. Krähenbühl, I. Köpping, T.A. Larsen, K.M. Udert, A novel approach for stabilizing fresh urine by calcium hydroxide addition, Water Res. 95 (2016) 361–369, https://doi.org/10.1016/j.watres.2016.03.007.
[24] R.C. Hoseney, K.F. Finney, Spectrophotometric determination of urea, Thiourea, and certain of their substitution products with p-Dimethylaminobenzaldehyde and Diacetylmonoxime, Anal. Chem. 36 (1964) 2145–2148, https://doi.org/10.1021/ac60217a034.
[25] L. Koók, B.K. Nagy, I. Nyirő-Kósa, S. Kovács, J. Zitka, M. Otmar, P. Bakonyi, N. Nemestóthy, K. Bélafi-Bakó, Simultaneous urea and phosphate recovery from synthetic urine by electrochemical stabilization, Membranes (Basel) 13 (2023) 699, https://doi.org/10.3390/membranes13080699.
[26] E. Zikmund, K.Y. Kim, B.E. Logan, Hydrogen production rates with closely-spaced felt anodes and cathodes compared to brush anodes in two-chamber microbial electrolysis cells, Int. J. Hydrog. Energy 43 (2018) 9599–9606, https://doi.org/10.1016/j.ijhydene.2018.04.059.
[27] E.U. Fonseca, K.Y. Kim, R. Rossi, B.E. Logan, Improving microbial electrolysis stability using flow-through brush electrodes and monitoring anode potentials relative to thermodynamic minima, Int. J. Hydrog. Energy 46 (2021) 9514–9522, https://doi.org/10.1016/j.ijhydene.2020.12.102.
[28] P. Khongkliang, P. Kongjan, B. Utarapichat, A. Reungsang, S. O-Thong, Continuous hydrogen production from cassava starch processing wastewater by two-stage thermophilic dark fermentation and microbial electrolysis, Int. J. Hydrog. Energy 42 (2017) 27584–27592, https://doi.org/10.1016/j.ijhydene.2017.06.145.
[29] R. Cardeña, J. Žitka, L. Koók, P. Bakonyi, L. Pavlovec, M. Otmar, N. Nemestóthy, G. Buitrón, Feasibility of quaternary ammonium and 1,4-diazabicyclo[2.2.2]octane-functionalized anion-exchange membranes for biohydrogen production in microbial electrolysis cells, Bioelectrochemistry 133 (2020) 107479, https://doi.org/10.1016/j.bioelechem.2020.107479.
[30] B.E. Logan, R. Rossi, A. Ragab, P.E. Saikaly, Electroactive microorganisms in bioelectrochemical systems, Nat. Rev. Microbiol. 17 (2019) 307–319, https://doi.org/10.1038/s41579-019-0173-x.
[31] G. Beretta, M. Daghio, A.E. Tofalos, A. Franzetti, A.F. Mastorgio, S. Saponaro, E. Sezenna, Microbial assisted hexavalent chromium removal in bioelectrochemical systems, Water (Switzerland) 12 (2020) 466, https://doi.org/10.3390/w12020466.
[32] S.G. Barbosa, L. Peixoto, A. Ter Heijne, P. Kuntke, M.M. Alves, M.A. Pereira, Investigating bacterial community changes and organic substrate degradation in microbial fuel cells operating on real human urine, Environ. Sci. (Camb) 3 (2017) 897, https://doi.org/10.1039/c7ew00087a.
[33] B. Krajewska, S. Ciurli, Jack bean (Canavalia ensiformis) urease. Probing acid–base groups of the active site by pH variation, Plant Physiol. Biochem. 43 (2005) 651–658, https://doi.org/10.1016/j.plaphy.2005.05.009.
[34] H. Ray, D. Saetta, T.H. Boyer, Characterization of urea hydrolysis in fresh human urine and inhibition by chemical addition, Environ. Sci. (Camb) 4 (2018) 87–98, https://doi.org/10.1039/c7ew00271h.
[35] H.L. Barazorda-Ccahuana, B. Gómez, F. Mas, S. Madurga, Effect of pH on the supramolecular structure of helicobacter pylori urease by molecular dynamics simulations, Polymers (Basel) 12 (2020) 2713, https://doi.org/10.3390/polym12112713.
[36] L. Mazzei, M. Cianci, S. Benini, S. Ciurli, The impact of pH on catalytically critical protein conformational changes: the case of the urease, a nickel enzyme, chemistry – a, European Journal 25 (2019) 12145–12158, https://doi.org/10.1002/chem.201902320.
[37] M. James, W.A. Mitch, Electrochemical generation of hydroxide for precipitative water softening, ACS ES and T Water 2 (2022) 2677–2685, https://doi.org/10.1021/acsestwater.2c00451.
[38] K.R. Lynn, Kinetics of base-catalyzed hydrolysis of urea, J. Phys. Chem. 69 (1965) 687–689, https://doi.org/10.1021/j100886a516.
[39] G. Estiu, K.M. Merz, The hydrolysis of urea and the proficiency of urease, J. Am. Chem. Soc. 126 (2004) 6932–6944, https://doi.org/10.1021/ja049327g.
[40] R.C. Warner, The kinetics of the hydrolysis of urea and of arginine, J. Biol. Chem. 142 (1942) 705–723, https://doi.org/10.1016/s0021-9258(18)45072-7.
[41] W. Chin, W. Kroontje, Urea hydrolysis and subsequent loss of Ammonia, Soil Sci. Soc. Am. J. 27 (1963) 316–318, https://doi.org/10.2136/sssaj1963.03615995002700030030x.
[42] Y. Lei, Z. Zhan, M. Saakes, R.D. van der Weijden, C.J.N. Buisman, Electrochemical recovery of phosphorus from acidic cheese wastewater: feasibility, quality of products, and comparison with chemical precipitation, ACS ES&T, Water 1 (2021) 1002–1013, https://doi.org/10.1021/acsestwater.0c00263.
[43] H. Liu, X. Li, H. Yao, P. Sun, Enhanced strategies for phosphate recovery from urine by magnesium galvanic process, Water Res. 245 (2023) 120669, https://doi.org/10.1016/j.watres.2023.120669.
[44] L. Xu, R. Ding, Y. Mao, S. Peng, Z. Li, Y. Zong, D. Wu, Selective recovery of phosphorus and urea from fresh human urine using a liquid membrane chamber integrated flow-electrode electrochemical system, Water Res. 202 (2021) 117423, https://doi.org/10.1016/j.watres.2021.117423.
[45] Z. Wang, Z. He, Electrochemical phosphorus leaching from digested anaerobic sludge and subsequent nutrient recovery, Water Res. 223 (2022) 118996, https://doi.org/10.1016/j.watres.2022.118996.
[46] Y. Lei, E. Geraets, M. Saakes, R.D. van der Weijden, C.J.N. Buisman, Electrochemical removal of phosphate in the presence of calcium at low current density: precipitation or adsorption? Water Res. 169 (2020) 115207 https://doi.org/10.1016/j.watres.2019.115207.
[47] M. Oliot, S. Galier, H.R. de Balmann, A. Bergel, Ion transport in microbial fuel cells: key roles, theory and critical review, Appl. Energy 183 (2016) 1682–1704, https://doi.org/10.1016/j.apenergy.2016.09.043.
[48] T.H.J.A. Sleutels, H.V.M. Hamelers, R.A. Rozendal, C.J.N. Buisman, Ion transport resistance in microbial electrolysis cells with anion and cation exchange membranes, Int. J. Hydrog. Energy 34 (2009) 3612–3620, https://doi.org/10.1016/j.ijhydene.2009.03.004.
[49] R.A. Rozendal, H.V.M. Hamelers, C.J.N. Buisman, Effects of membrane cation transport on pH and microbial fuel cell performance, Environ. Sci. Technol. 40 (2006) 5206–5211, https://doi.org/10.1021/es060387r.
[50] A. Ter Heijne, H.V.M. Hamelers, V. De Wilde, R.A. Rozendal, C.J.N. Buisman, A bipolar membrane combined with ferric iron reduction as an efficient cathode system in microbial fuel cells, Environ. Sci. Technol. 40 (2006) 5200–5205, https://doi.org/10.1021/es0608545.
[51] C.Y. Sousa, A. Fernandes, A. Amaro, M.J. Pacheco, L. Ciríaco, A. Lopes, Electrochemical recovery of phosphorus from simulated and real wastewater: effect of investigational conditions on the process efficiency, Sustainability 15 (2023) 16556, https://doi.org/10.3390/su152416556.
[52] Z. Wang, Z. He, Electrochemical phosphorus leaching from digested anaerobic sludge and subsequent nutrient recovery, Water Res. 223 (2022) 118996, https://doi.org/10.1016/j.watres.2022.118996.
[53] Z. Wang, F. Liu, Z. He, Electrochemical phosphorus release and recovery from wastewater sludge: a review, Crit. Rev. Environ. Sci. Technol. 53 (2023) 1359–1377, https://doi.org/10.1080/10643389.2023.2172928.